

<https://doi.org/10.1038/s42003-025-08182-w>

Inhibiting inositol transport disrupts metabolite profiles and mimics heat stress in a model cnidarian-Symbiodiniaceae symbiosis




Lauren D. Turner¹, Jean-Baptiste Raina ^{1,2}, Unnikrishnan Kuzhiumparambil¹, Kittikun Songsomboon¹ & Jennifer L. Matthews ¹ 

The nutrient exchange between corals and their symbiotic microalgae (Symbiodiniaceae) is vital for coral survival. Disruptions in this mutualistic relationship, often due to stress-induced dysbiosis, contribute significantly to coral mortality and reef decline globally. Dysbiosis is associated with substantial shifts in various metabolites, notably a rise in inositol, a sugar alcohol, though its role in coral-algae interactions remains unclear. Using a cnidarian model, we identify Symbiodiniaceae as the main source of inositol, with *myo*- and *scyllo*-inositol being the dominant forms under normal conditions. During heat stress, *scyllo*-inositol levels increase by 1.8 times in symbiotic hosts, and up to 26 times in cultured Symbiodiniaceae (*Breviolum minutum*). Meanwhile, *myo*-inositol decreases in host tissues but doubles within Symbiodiniaceae, indicating altered nutrient-sharing or stress signalling. In contrast, no changes are observed in aposymbiotic cnidarians (without Symbiodiniaceae). Additionally, inhibiting inositol production and transport in symbiotic tissues disrupts metabolite profiles, mimicking effects seen under heat stress, suggesting that inositol transport is crucial for maintaining metabolic balance and nutrient exchange. These findings reveal that disruptions in inositol dynamics play a critical role in stress responses, offering insights into dysbiosis mechanisms driving coral reef crises.

Heat-induced bleaching reduces the density and function of Symbiodiniaceae in coral tissues, thereby diminishing or ceasing autotrophic input from these symbionts^{1,2}. A decline in the relative availability of glucose, a major photosynthetic product transferred from *in hospite* Symbiodiniaceae to the cnidarian host³, in coral tissues is one of the first metabolic symptoms demonstrated by stress^{2,4,5}. As glucose is crucial for central metabolic processes such as glycolysis, its depletion severely impacts coral health and survival, forcing the host to mobilise stored energy reserves to support vital functions^{2,3,6}. Also under heat stress, inositol concentrations can increase dramatically up to 4-fold in Symbiodiniaceae while *in hospite*, 11-fold in *Exaiptasia pallida* host tissues, 13-fold in *Acropora tenuis* host tissues, and 100-fold in cultured Symbiodiniaceae^{4,5,7}. Changes in the glucose and inositol levels, among other metabolic shifts in the host, are a hallmark of dysbiosis (i.e., functional and physical breakdown of the cnidarian-Symbiodiniaceae symbiosis), ultimately contributing to coral bleaching,

which reduces immunity⁸, hampers reproductive rates^{9,10}, and increases mortality¹¹. However, the underlying mechanisms affecting the functional exchange of metabolites between host and symbiont remain unclear.

Inositol is a very small, polar molecule with nine isometric forms. Six of these stereoisomers are naturally produced (*myo*-, *D-chiro*-, *L-chiro*-, *scyllo*-, *muco*-, *neo*), with *myo*-inositol being the most abundant in nature, as it can be synthesised and used by many Archaea, bacteria, and all eukaryotes^{12,13}. *Myo*-inositol forms a structural basis for various lipids and phosphates^{14,15} such as the phosphoinositide signalling pathway involving phosphatidylinositol (PI), which are important membrane lipids and secondary messengers in eukaryotes^{16,17}. The role of inositol and its various isomers has been heavily studied in other organisms. For example, *myo*-inositol is the primary source of carbon for some yeast species¹⁸, and plays a role in the virulence of the fungus *Cryptococcus neoformans* through acting as a carbon source and/or a signalling molecule¹⁹. In animal-bacteria symbioses (e.g., the

¹Climate Change Cluster, University of Technology Sydney, Sydney, Ultimo 2007 NSW, Australia. ²PSL Université Paris: EPHE-UPVD-CNRS, USR 3278 CRILOBE, Université de Perpignan, 52 Avenue Paul Alduy, 66860 Perpignan, CEDEX, France.  e-mail: Jennifer.Matthews@uts.edu.au

Hawaiian bobtail squid-*Vibrio fischeri* symbiosis), *myo*-inositol enhances phagocytosis and therefore has a role in regulating bacterial abundances within the host^{20,21}. Furthermore, *Arabidopsis* secretes *myo*-inositol, a compound essential for the growth and function of *Bacillus megaterium*, which in turn promotes plant growth²². Disrupting the secretion of *myo*-inositol significantly reduces the colonisation of this bacterium, highlighting its critical role in the plant-microbe interaction and dysbiosis. D-*chiro*-inositol is an intermediate of pinitol catabolism, which plays a role in the ability of *Sinorhizobium meliloti*, the nitrogen-fixing symbiont of alfalfa, to compete for nodule occupancy²³.

Beyond heat stress, previous studies have shown that inositol levels in cnidarians are influenced by various biotic and abiotic factors such as light, salinity, pathogen presence, and associations with suboptimal symbionts^{4,6,7,24,25} (Table 1). These findings suggest a pivotal role for inositols in cnidarian-Symbiodiniaceae stress responses, which may be due to their functions as osmoprotectants, antioxidants, and regulators of key signalling pathways such as PI^{4,26,27}. In addition to the onset of host-symbiont interactions^{28,29}, PI signalling is known to regulate various stress- and growth-related pathways through the coordinated activities of isoforms, enzymes, kinases, and phosphatases, functioning to adapt growth and stress responses in plants³⁰. PI signalling, important in parasite-host infection^{31–33} may similarly influence the establishment and maintenance of mutualisms^{28,29}. Several proteins involved in the PI signalling pathway are differentially expressed in both cnidarian hosts (including *E. diaphana*^{30,34,35}) and Symbiodiniaceae (including *Breviolum*^{30,36}) in response to symbiotic states^{4,6,34–39}. In *B. minutum*, transcriptional changes in PI signalling components point to broader roles for this pathway in thermal response³⁸. Phosphoinositides (PIPs), which are PI phosphates, are precursors to secondary messengers known as inositol polyphosphates (IPs). Inositol monophosphate (IP) and inositol biphosphate (IP₂) levels increased in *Pocillopora acuta* adapted to high salinity mangrove environments during heat stress⁴⁰, though IP decreased by 0.7-fold in temperate Pocilloporid corals under temperature stress conditions⁴¹. Yet, the role of inositols in cnidarian-Symbiodiniaceae stress responses remains unclear.

Inositol cotransporters, such as proton-coupled *myo*-inositol transporters (HMIT), are upregulated in symbiotic cnidarians compared to those without Symbiodiniaceae (aposymbiotic)⁶. Similarly, the Na⁺-*myo*-/*scyllo*-inositol co-transporter SMIT1 and the *myo*-/*chiro*-inositol transporter SMIT2 are exclusively expressed in symbiotic *E. diaphana*³⁵. While HMIT and SMIT primarily mediate the transport of *myo*-inositol, they can also transport other inositols. For example, *scyllo*-inositol can induce similar fluxes in both SMIT1⁴² and HMIT⁴³, while SMIT2 can accept *chiro*-inositol⁴⁴. Additionally, these transporters can also mediate the movement

of monosaccharides, such as glucose, fructose, and xylose^{34,45,46}. The shifts in inositol and glucose levels during stress², coupled with the symbiosis-dependent expression of these transporters³⁵, suggest that inositol transport plays a crucial role in maintaining a functional symbiosis. Therefore, understanding the dynamics of inositol transport during dysbiosis could offer significant insights into the breakdown of metabolite exchange and the mechanistic disruption of the cnidarian-Symbiodiniaceae symbiosis. We employed advanced techniques in chemical analysis and pharmacology to examine inositol dynamics in a model cnidarian-Symbiodiniaceae symbiosis. We hypothesise that inositol isoforms are actively produced and exchanged between the partners and that stress profoundly alters their production and dynamics, potentially impacting the stability of the symbiotic relationship.

Results and discussion

Scyllo-inositol is the main isoform produced by Symbiodiniaceae and shared to cnidarian hosts

Previous studies have reported the detection of *myo*-, *chiro*-, *scyllo*-inositols and various inositol phosphates in *Exaiptasia diaphana* and coral tissues^{5,24,41,47}. In cultured Symbiodiniaceae, two different inositol stereoisomers have been detected, but were not distinguished^{7,25}. Here, we employed targeted Gas Chromatography–Mass Spectrometry (GC–MS) to quantify the concentration of *myo*-, *chiro*-, *scyllo*-inositols in symbiotic cnidarians (*Exaiptasia diaphana*) and their microalgal symbionts.

We detected *myo*- and *scyllo*-inositol in cultured Symbiodiniaceae (*Breviolum minutum*) and *B. minutum* in hospite (Fig. 1, Supplementary Data 1), but not *chiro*-inositol (Supplementary Data 1). Over the light cycle (measured at mid- (6 h; T1) and end-light cycle (9 h; T2)), intracellular concentrations of *scyllo*-inositol consistently exceeded those of *myo*-inositol in cultured *B. minutum* (One-sided *T*-test, T1: *T* = 4.84, *df* = 8, *p* < 0.01; T2: *T* = 2.11, *df* = 8, *p* = 0.03; Fig. 1A, C, Supplementary Data 1). This result was unexpected, given that *scyllo*-inositol isomer is usually rare in nature^{13,16,48}. We also identified an ortholog for *scyllo*-inositol-2-dehydrogenase, the enzyme involved in the conversion of *scyllo*-inositol to *scyllo*-inositol, in *B. minutum*, *Cladocodium goreau*, and *Durusdinium trenchii* genomes (Supplementary Data 2), suggesting that the ability to synthesise this isomer is widespread in Symbiodiniaceae. By the end of the light cycle, *scyllo*-inositol levels were 2-fold higher than *myo*-inositol in cultured *B. minutum* (Fig. 1A, C, Supplementary Data 1). Both inositols reached their lowest abundance during the dark phase (T3; 12 h dark, 24 h total), with *myo*-inositol decreasing 3-fold and *scyllo*-inositol levels decreasing 7-fold (Fig. 1A, C, Supplementary Data 1). These two molecules were also detected in the spent medium of *B. minutum* cultures during mid-light cycle (but

Table 1 | Summary table of studies and their results that have observed inositol in cnidarians and/or Symbiodiniaceae during periods of stress

Specimen	Stressor	Change in abundance	Study
Aiptasia and Symbiodiniaceae	Heat stress	<i>Scyllo</i> - 11-fold increase in host	Hillyer et al. ⁵
		<i>Chiro</i> - 0.5-fold increase in host	
		<i>Scyllo</i> - 4-fold increase in symbiont	
Anemones	Increased depth	<i>Myo</i> - 2.6-fold increase	Yancey et al. ⁵²
		<i>Scyllo</i> - 1.5-fold increase	
Coral	Heat stress	<i>Chiro</i> - 13-fold increase in host	Hillyer et al. ⁴
		<i>Scyllo</i> - 1.25-fold increase in host	
Coral	Heat stress	<i>Scyllo</i> - 0.3-fold increase	González-Pech et al. ⁴¹
		<i>Myo</i> - 0.5-fold decrease	
		InsP – 0.7-fold increase	
Coral	Microplastic	No abundance data given	Lancôt et al. ⁴⁷
Symbiodiniaceae in culture	Heat stress and high light intensity	100-fold increase (no isomer distinguished)	Klueter et al. ⁷
Symbiodiniaceae in culture	Increased salinity	19-fold increase (no isomer distinguished)	Ochsenkühn et al. ²⁵

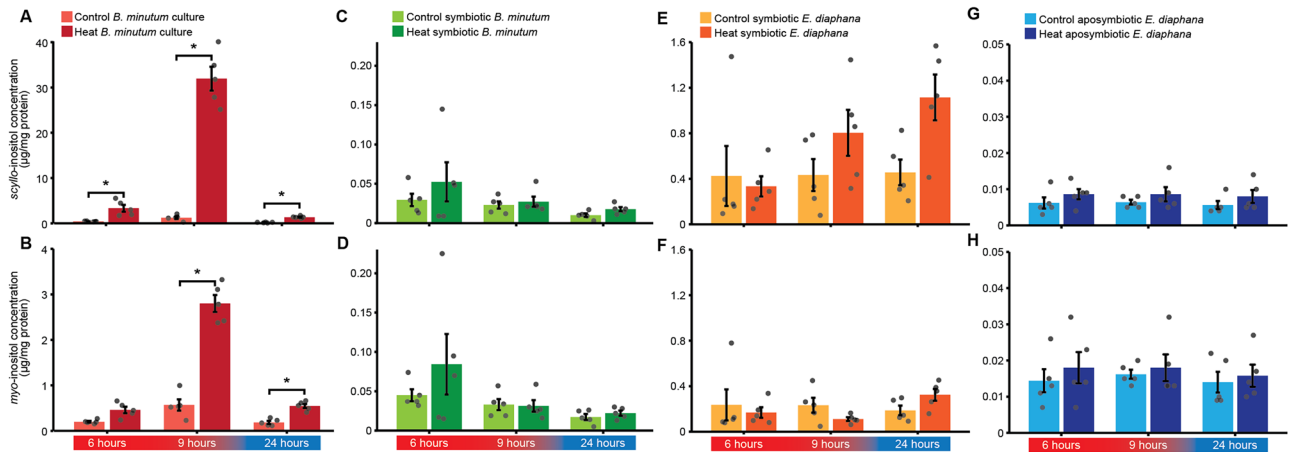


Fig. 1 | Absolute concentrations of inositol isoforms in cultured and in hospite Symbiodiniaceae (*Breviolum minutum*), and symbiotic and aposymbiotic cnidarians (*Euphyllia diaphana*), under control and heat-stressed conditions. Concentrations of *scyllo*-inositol (A, C, E, G) and *myo*-inositol (B, D, F, H) are

shown for *B. minutum* cultures (A, B), symbiotic *B. minutum* (C, D), symbiotic *E. diaphana* tissues (E, F), and aposymbiotic host tissues (G, H). Note: y-axes are scaled differently to increase readability. Data and statistical comparisons are provided in Supplementary Data 1 ($n = 5$ per treatment).

not in all samples) with concentrations 433 times (*myo*-inositol) and 1495 times (*scyllo*-inositol) lower than those measured intracellularly, but then became undetectable at the end of the light cycle (Supplementary Data 3). This result supports previous evidence of limited extracellular transport of inositol when not *in hospite*³.

E. diaphana is a model cnidarian frequently used to study coral-Symbiodiniaceae symbiosis, as it can be easily rendered aposymbiotic and maintained in this state indefinitely^{49–53}. Both *myo*- and *scyllo*-inositol were detected in aposymbiotic and symbiotic *E. diaphana* tissues (in symbiosis with *B. minutum*), while *chiro*-inositol was not detectable (Fig. 1B, D, Supplementary Data 1). Intracellular concentrations of both *myo*- and *scyllo*-inositol were significantly lower in *B. minutum* *in hospite* compared to cultured *B. minutum* cells across the light cycle (Tukey HSD, $p < 0.001$; Fig. 1B, D, Supplementary Data 1). While we cannot completely rule out a bacterial contribution to the inositol levels measured in culture, previous evidence shows that removing bacteria increases the inositol levels per Symbiodiniaceae cell⁵⁴. This suggests that the observed differences in inositol concentrations between culture and *in hospite* conditions are more likely driven by their association with the cnidarian host rather than their bacterial symbionts. In symbiotic *E. diaphana* tissues, *scyllo*-inositol concentrations were 73.8-fold higher on average than in aposymbiotic tissues and were 2.1-fold higher on average than *myo*-inositol across the light cycle (Fig. 1, Supplementary Data 1). Conversely, in aposymbiotic anemones, *myo*-inositol concentrations were 2.45-fold higher on average than *scyllo*-inositol (Fig. 1, Supplementary Data 1). *E. diaphana* possesses genes involved in *myo*-inositol biosynthesis (e.g., inositol monophosphatase 1 and inositol-3-phosphate synthase)^{13,49} and can convert *myo*-inositol to the intermediate *scyllo*-inosose (through the enzyme inositol dehydrogenase). However, current genomic data suggest that *scyllo*-inositol-2-dehydrogenase genes are absent in the genome of *E. diaphana*⁵⁵ (Supplementary Data 2), as well as the genomes of corals *Acropora millepora*⁵⁶ and *A. digitifera*⁵⁷. Therefore, as *scyllo*-inositol is the most abundant isoform in Symbiodiniaceae cells in culture but is significantly reduced when *in hospite* (Tukey HSD, $p < 0.001$; Supplementary Data 1), and this compound is almost two orders of magnitude higher in symbiotic compared to aposymbiotic *E. diaphana*, we conclude that *E. diaphana* obtain most of this metabolite from its resident Symbiodiniaceae.

Heat stress triggers an increase in inositol isoform concentrations

We examined the effects of acute heat stress⁵⁸ (Supplementary Fig. 1) on the abundance of inositol stereoisomers in cultured *B. minutum* and symbiotic and aposymbiotic *E. diaphana*. Heat stress significantly reduced the

maximum quantum yield of PSII (F_v/F_m) in *B. minutum* cultures (One-sided T -test, $t = 19.308$, $df = 8$, $p < 0.001$; Supplementary Data 4), confirming physiological stress⁵⁹. Concomitantly, *myo*-inositol increased significantly in cultured *B. minutum* under heat stress, with concentrations reaching 4.9 times higher than in control cultures (Fig. 1C, Supplementary Data 1). During recovery, levels remained elevated (2.9-fold over controls) (Fig. 1C, Supplementary Data 1). Actinidia plants follow a similar pattern under salinity stress, where *myo*-inositol can increase linearly as stress intensifies before decreasing after the removal of stress⁶⁰. These observations point to a broader role for *myo*-inositol in managing environmental stress across taxa.

Interestingly, *scyllo*-inositol concentrations increased 7.3-fold in heat-stressed *B. minutum* cultures and were 26-fold higher than controls at peak heat stress (Fig. 1A). During recovery, *scyllo*-inositol levels declined but remained 7 times higher than in controls (Fig. 1A, Supplementary Data 1). The rapid and substantial increase suggests that *scyllo*-inositol plays a key role in responding to temperature stress, potentially as an osmoprotectant or stabiliser of cellular function, as seen in other marine organisms^{61–64}.

In symbiotic *E. diaphana*, we observed an average decline in photosynthetic efficiency in heat-exposed anemones compared to controls; however, this reduction was not statistically significant (Supplementary Data 5). Interestingly, *chiro*-inositol was only detected in heat-stressed host extracts, although the concentration of this compound was significantly lower than the other two stereoisomers throughout (Tukey HSD, $p < 0.001$; Supplementary Data 1). *Chiro*-inositol has previously been reported to increase in heat-stressed *E. diaphana* and *A. tenuis* tissues, and similarly, was not detected in Symbiodiniaceae *in hospite*^{4,5}. *Chiro*-inositol is present in other symbioses, for example between soybean and bacteroids⁶⁵, where it is used as a carbon source along with *myo*-inositol by the symbiotic bacteria⁶⁵.

Intracellular *scyllo*-inositol concentrations in heat-exposed symbiotic host tissues doubled at peak heat exposure compared to controls and continued to increase throughout the recovery period, whereas levels in control tissues remained stable throughout (Fig. 1, Supplementary Data 1). In *in hospite* *B. minutum*, *scyllo*-inositol levels doubled at the onset of heat exposure but returned to control levels during peak heat exposure and recovery (Fig. 1, Supplementary Data 1). Meanwhile, in aposymbiotic *E. diaphana*, *scyllo*-inositol levels did not change in heat-exposed or control conditions (Fig. 1, Supplementary Data 1). This suggests that *scyllo*-inositol may play a role in the early stages of heat adaptation in symbiotic cnidaria, particularly in host tissues. As this response was dependent on symbiotic state, it further supports a role of this metabolite in Cnidaria-Symbiodiniaceae signalling and symbiotic function.

In contrast, *myo*-inositol followed a more complex pattern, with its dynamics likely reflecting shifts in metabolic priorities between host and symbiont under stress. In *E. diaphana*, we observed that *myo*-inositol levels decreased in host tissues during early heat exposure but doubled in *in hospite* *B. minutum* (Fig. 1D). This suggests a potential disruption in metabolite translocation between symbiont and host, possibly indicating shifts in nutrient-sharing dynamics or stress signalling during early heat stress^{4,30}. After recovery, *myo*-inositol levels in symbiotic host tissues surged, while they returned to control levels in the *in hospite* *B. minutum*, possibly reflecting restored metabolite transfer and signalling from the symbionts.

Blocking inositol transport leads to metabolic signatures undistinguishable from heat stress

We pharmacologically inhibited inositol by dosing symbiotic *E. diaphana* with lithium, and assessed symbiont photophysiology, and the metabolite profiles of separated host and symbionts using GC-MS metabolite profiling. Lithium ions inhibit inositol monophosphatase (IMPase), which converts IP to inositol, and indirectly inhibit the activity and expression of SMIT transporters⁶⁶. After optimising lithium concentrations in cultured *B. minutum* to determine the minimum effective dose that alters *scyllo*- and *myo*-inositol levels (Supplementary Data 5; Supplementary Fig. 2), we exposed symbiotic *E. diaphana* to acute heat stress⁵⁸, with or without 0.1 mM lithium for 96 h. Heat stress significantly reduced algal photosynthetic efficiency (F_v/F_m ; Repeated Measure ANOVA, $p < 0.05$; Supplementary Data 6), while lithium exposure at 0.1 mM under control conditions had no effect (Repeated Measure ANOVA, $p = 0.13$; Supplementary Data 6). The metabolite profiles of symbiotic *E. diaphana* (Supplementary Data 7) and *B. minutum* symbionts (Supplementary Data 8) under control conditions without lithium were significantly different from those subjected to lithium dosing and/or heat stress (PERMANOVA; $p < 0.05$, Fig. 2, Supplementary Data 9). There is some overlap in the metabolite profiles of heat with lithium and control without lithium symbiont samples, suggesting that lithium may influence symbiont metabolism independently of heat stress. Additionally, heatmap clustering shows closer alignment in 3 out of 5 host samples and 4 out of 5 symbiont samples between these treatments. This could indicate a potential “rescue effect,” where lithium mitigates heat stress signals from the host to the symbiont,

preserving symbiosis. However, the high variability within the heat with lithium treatment and statistical test results suggests that any such effect is inconsistent.

Interestingly, lithium exposure at control temperatures produced metabolite profiles highly similar to those observed in both heat-stressed (PERMANOVA; $p = 0.70$) and heat-plus-lithium-treated *E. diaphana* (PERMANOVA; $p = 0.75$) (Fig. 2, Supplementary Data 9). The resemblance between the metabolite profiles of heat-stressed *E. diaphana* (not exposed to lithium) and control *E. diaphana* treated with lithium supports a functional role of inositol in maintaining optimal symbiosis and provides mechanistic insight (e.g., via inhibition of inositol co-transport) into the breakdown of this symbiosis under stress.

Individual metabolite analysis revealed that *myo*-inositol significantly decreased in *E. diaphana* host tissues following lithium exposure and heat stress (ANOVA, $p < 0.05$, Fig. 3A, Supplementary Data 10). This is consistent with the blocking of host SMIT transporters in the heat and lithium-exposed anemones, including SMIT2, which transport both *myo*- and *chiro*-inositols. *Chiro*-inositol competes with *myo*-inositol in SMIT2-mediated transport and has been used as a specific inhibitor of SMIT2, but not SMIT1⁴⁸. Converse to *myo*-inositol, *chiro*-inositols significantly increased in *E. diaphana* host tissues following both lithium exposure under control temperatures, and heat stress with and without lithium (ANOVA, $p < 0.05$, Fig. 3, Supplementary Data 10). *Chiro*-inositols were previously undetected in *E. diaphana* under control conditions (Supplementary Data 1), therefore, the inhibition of the SMIT2 transporters under the control temperatures could reduce the effective export of the *chiro*-inositol isoforms, leading to their intracellular accumulation.

Scyllo-inositol levels varied significantly across all treatments, with the highest concentrations observed in heat-stressed anemones without lithium, and the lowest in the control group, consistent with previous findings (ANOVA, $p < 0.05$, Supplementary Fig. 3, Supplementary Data 1 and 10). Notably, both the heat-stressed and heat-plus-lithium-treated anemones exhibited significantly higher *scyllo*-inositol concentrations than the lithium-treated control group, suggesting that these transporters may not be the sole source of *scyllo*-inositol. This also points to the potential mobilisation of stored *scyllo*-inositol within the anemones under stress conditions. For example, heat stress and lithium can affect the PI

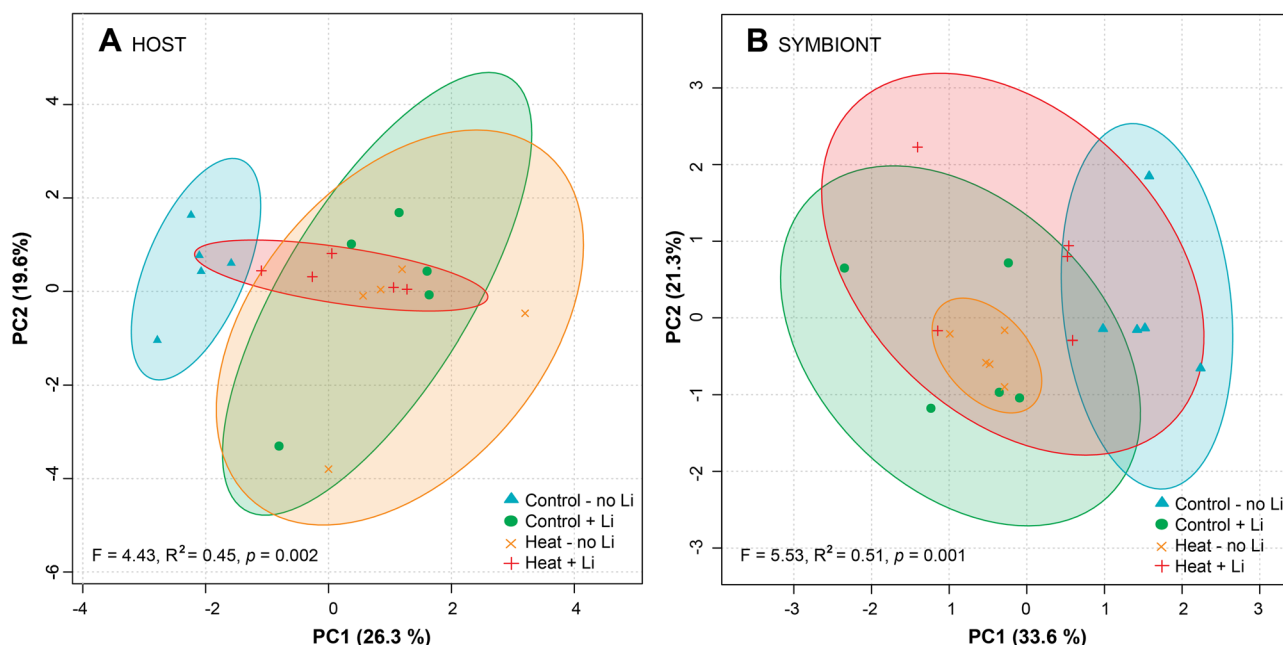


Fig. 2 | Principal Component Analysis (PCA) of *E. diaphana* and *B. minutum* metabolite profiles under heat- and lithium-exposure. PCA reveals the differences in the metabolite profiles of *E. diaphana* host (A) and *Breviolum minutum*

(B) symbionts following exposure to heat and lithium treatments. Data are provided in Supplementary Data 8 and 9. PERMANOVA statistics are provided as inserts and are detailed in Supplementary Data 9.

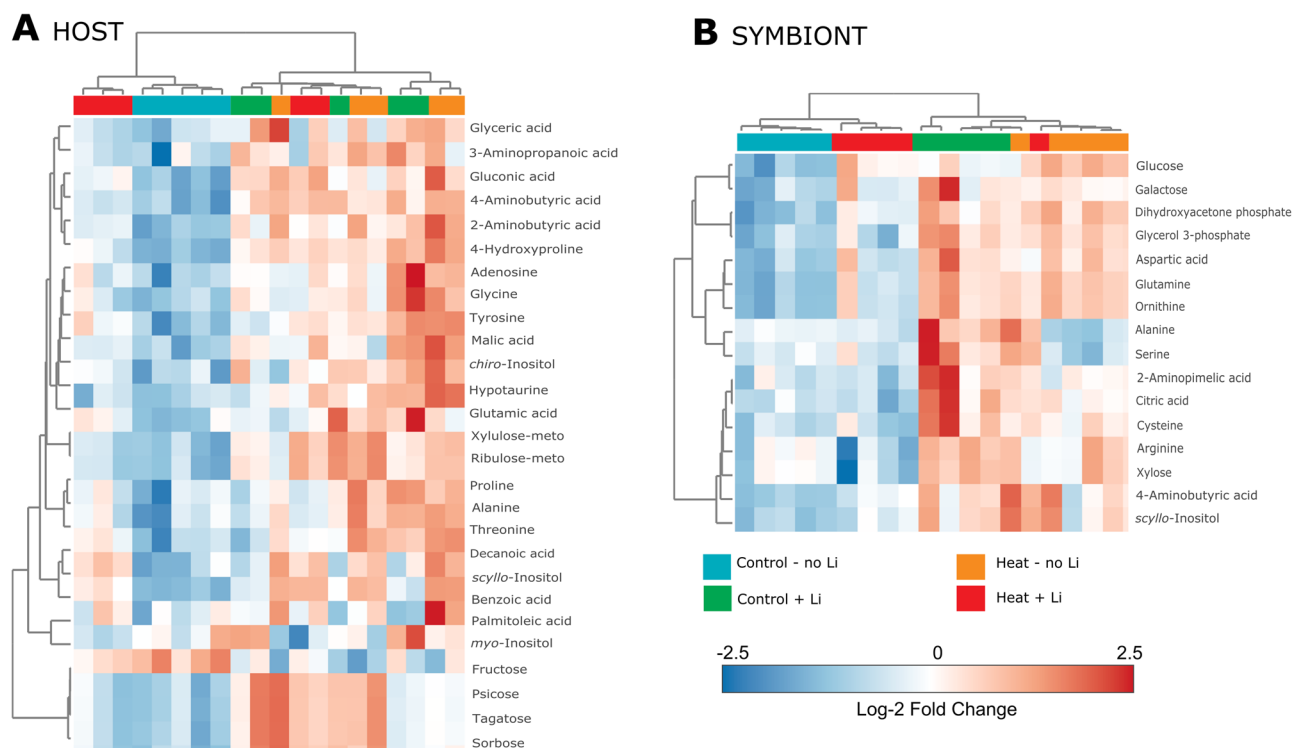


Fig. 3 | Heatmap visualisation of significantly altered metabolites in *E. diaphana* and *B. minutum* under heat and lithium exposure. Significantly different metabolites (ANOVA, $p < 0.05$) between heat- and lithium-exposed treatments in

E. diaphana (A) and *B. minutum* symbionts (B). Metabolite intensities are log₂ fold change. Data is available in Supplementary Data 10.

signalling system by elevating inositol monophosphate (IP) levels, followed by phosphoinositols accumulation⁶⁷, which might lead to the elevated *scyllo*-inositol levels.

Besides the inositols, the abundance of 27 other metabolites was significantly altered by heat and lithium exposure in the host tissues (ANOVA, $p < 0.05$, Fig. 3A, Supplementary Data 10). Most of these metabolites (25/27) were significantly different between the controls with and without lithium, and between controls and heat-exposed anemones without lithium (ANOVA, $p < 0.05$, Supplementary Data 10). This indicates that heat stress elicits a response in *Exaiptasia* similar to that triggered by lithium exposure and supports the hypothesis that disruptions in inositol translocation play a role in the organism's response to heat stress.

While glucose abundance remained unchanged, gluconic acid, which is enzymatically formed from glucose via glucose oxidase (a process that generates hydrogen peroxide), was elevated in both heat and lithium treatments compared to controls (ANOVA, $p < 0.05$, Fig. 3A, Supplementary Data 10). Gluconic acid, therefore, serves as a marker of oxidative stress, further supporting that similar stress-related mechanisms are triggered when these transporters are blocked.

Interestingly, palmitoleic acid (C16:1) was the only metabolite significantly higher in the control group compared to the treated groups. This fatty acid is crucial for the synthesis of C16 polyunsaturated fatty acids in corals, and both palmitic acid (C16:0) and palmitoleic acid are major components of total lipids in both cnidarians and Symbiodiniaceae²⁴. Additionally, several intermediates of fatty acid metabolism were more abundant in the heat and lithium-treated anemones (Fig. 3A, Supplementary Data 10), suggesting an upregulation of lipid metabolism and mobilisation of stored energy⁴. This shift away from central metabolism further underscores the similarity in metabolic stress and dysfunction caused by inositol transporter inhibition and heat exposure.

Scyllo-inositol concentrations were the only inositols affected in the symbiont cells, showing increased abundance under both heat and lithium exposure (ANOVA, $p < 0.05$, Fig. 3B, Supplementary Data 10). Notably, glucose and galactose levels also increased in the lithium and heat-exposed

symbiont cells compared to the controls (ANOVA, $p < 0.05$, Fig. 3B, Supplementary Data 10), possibly due to a failure in translocation to the host, leading to their accumulation within the symbiont². Similarly, several metabolites involved in the urea cycle, such as ornithine, arginine, and glutamine, were more abundant in symbiont cells under lithium and heat stress (ANOVA, $p < 0.05$, Fig. 3B, Supplementary Data 10). This finding is particularly important considering recent evidence highlighting the importance of nitrogen cycling during nutrient dysbiosis^{1,68}. Compared to cultured cells, *in hospite* *B. minutum* shows an upregulation of phosphatidylinositol 4-phosphate 5-kinase (PI4P5K) activity³⁰, which plays an important role in endosomal trafficking. This could reflect an increased demand for vesicle transport after colonisation of a host, underscoring a role for PI signalling and nutrient transfer in the regulation of the symbiosis^{30,39}.

Conclusions

The evidence presented here suggests that inositols play a key role in nutrient exchange and symbiosis function within cnidarian-Symbiodiniaceae symbioses, with changes in inositol dynamics potentially serving as markers of the early stages of dysbiosis under heat stress (Fig. 4). Inositol transport could play a role in regulating the PI signalling pathways in the cnidarian-Symbiodiniaceae symbiosis^{30,34}, as *myo*-inositol serves as a precursor for these pathways (including the PI signalling system and the inositol phosphate metabolism pathways) and *scyllo*-inositol can be converted into *myo*-inositol (Fig. 4). Inositol may also function as an alternative carbon source in the symbiosis, as observed in many bacteria, plants, and fungi, though this function has not been observed as such in metazoans¹⁶. Beyond its metabolic role, inositol also acts as an antioxidant and compatible solute, stabilising cellular proteins under environmental stressors such as heat and high salinity. Many eukaryotes across diverse environments use inositols and inositol-derived cyclitols as compatible solutes for cytoprotection. For example, hyperthermophilic archaea from marine hydrothermal vents accumulate di-*myo*-inositol phosphate and K⁺ to withstand extreme temperatures and salinities⁶², while *myo*-inositol is widely used as a feed additive in aquaculture to promote growth and enhance antioxidant capacity^{69,70}.

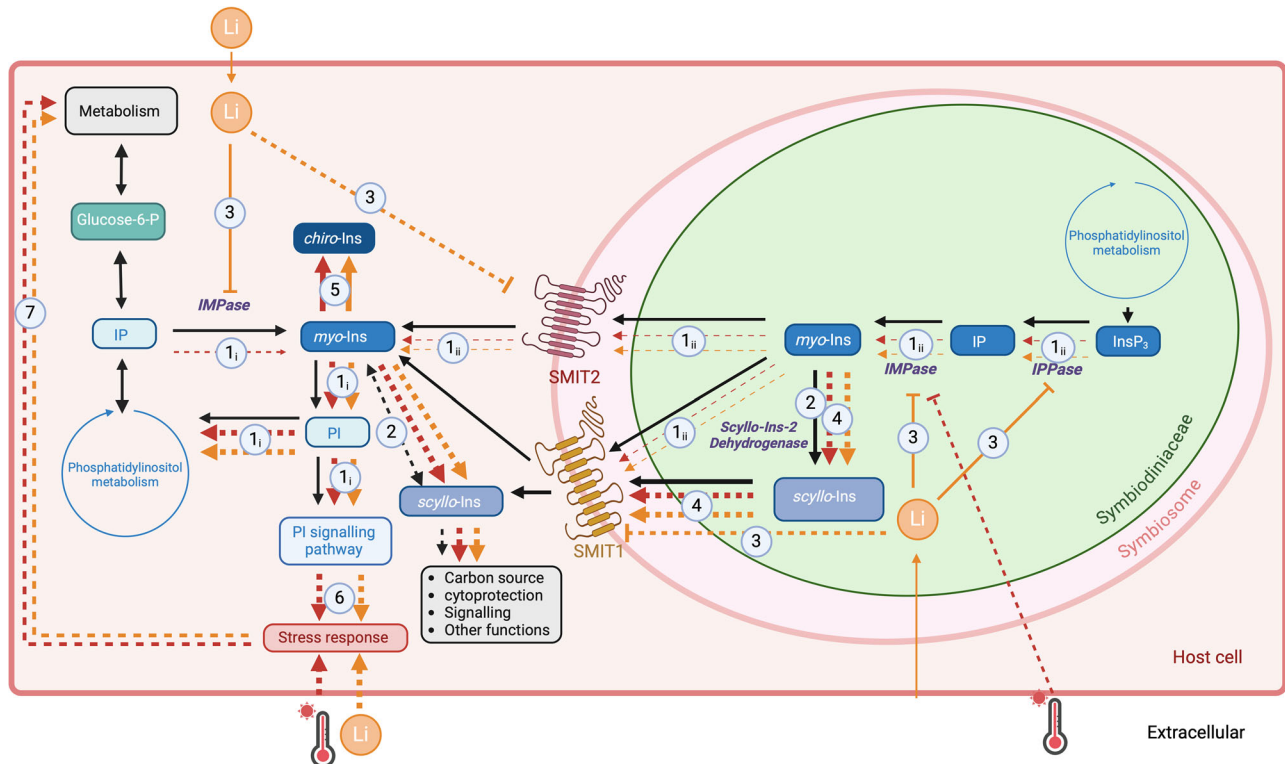


Fig. 4 | Schematic representation of the production of inositols and hypothesised pathway activity under lithium and heat stress. Arrow thickness indicates observed pathway activity, while colours denote different conditions: control (black), heat stress (red), and lithium exposure (orange). Solid arrows represent established pathways, whereas dotted lines indicate hypothesised pathways based on the current data. (1) Under normal conditions, *myo*-inositol is synthesised by host cells and translocated from the symbiont via SMIT1/2 and HMIT transporters (not shown). Under heat and lithium stress, *myo*-inositol levels in the host decrease, potentially due to: (i) reduced synthesis or diversion into phosphatidylinositol (PI) metabolism and signalling within host tissues, or (ii) reduced translocation from the symbiont, possibly caused by decreased synthesis, mobilisation from stored sources, or increased conversion to *scyllo*-inositol by Symbiodiniaceae (see point 4). (2) Under normal conditions, *scyllo*-inositol is synthesised and translocated by the symbiont, likely via SMIT1 transporters. In the host, *scyllo*-inositol may be converted

back to *myo*-inositol or serve other, yet unidentified, functions. (3) Lithium exposure inhibits IMPase and IPPase enzymes in both the host and symbiont, while also indirectly affecting SMIT1/2 function. This inhibition leads to a reduction in *myo*-inositol abundance in both host and symbiont cells. (4) Heat stress significantly decreases *myo*-inositol levels while increasing *scyllo*-inositol abundance in symbiont cells, suggesting an upregulation of *scyllo*-inositol synthesis. (5) *Chiro*-inositol is detected only in host tissues under heat stress and lithium exposure. (6) While not directly measured, inositol pathway alterations under stress may impact PI signalling, potentially triggering a stress response in the host. (7) Whether through inositol metabolism or other mechanisms, host responses to heat and lithium stress share common metabolic consequences. Glucose-6-P Glucose-6-Phosphate, IP inositol monophosphate, InsP₃ Inositol triphosphate, *myo*-Ins *myo*-inositol, *scyllo*-Ins *scyllo*-inositol, *chiro*-Ins *chiro*-inositol, Li Lithium, PI phosphatidylinositol. Created in BioRender. Matthews JL (2025) <https://BioRender.com/8eo2upj>.

Additionally, oral administration of *scyllo*-inositol has been shown to alleviate symptoms of Alzheimer's disease in mouse models by inhibiting amyloid beta (A β) aggregation⁷¹. These diverse protective functions highlight inositol's potential role in maintaining symbiosis. This study expands the known roles of inositols beyond animal-bacteria^{20,21} and plant-microbe²² interactions to include animal-microalgae symbioses, supporting the hypothesis that inositol's role in symbiotic interactions is evolutionarily conserved.

The similarity in metabolite profiles of heat-stress and inositol-inhibited host and symbiont cells provide important insights into the breakdown of symbiotic nutrient exchanges under stress. The accumulation of key metabolites like *scyllo*-inositol, glucose, and nitrogen-related compounds in symbiont cells suggests that disruptions in transport mechanisms lead to a metabolic imbalance that mirrors patterns of nutrient dysbiosis. This highlights the critical role of metabolite transport in maintaining coral-symbiont equilibrium and suggests that targeting these transport processes could be pivotal for understanding and mitigating stress-related breakdowns in coral symbioses. While the concentration changes in inositol during periods of stress is unknown for many species of coral, the increases during a variety of stressors, including temperature stress has been observed across *E. diaphana*, *Pocillopora acuta*, and members of the genus *Platygyra* and *Acropora*^{4,5,40,41,72}, making inositol a likely ubiquitous stress marker that could be used in future studies and management practices. To establish

inositol as a reliable biomarker for coral restoration strategies, future studies should assess inositol isoform expression across diverse coral genera and under various stressors, such as high light exposure⁷³. Integrating metabolite profiling with the analysis of transporter activity through transcriptomic⁶ or proteomic^{34,74} analyses could clarify the role of PI signalling in symbiosis and stress responses³⁰, helping to define the thresholds and timing of inositol-related stress signals. Once inositol biomarker responses are better characterised across coral genera, optimising in situ measurement techniques will be crucial. Methods such as the enzymatic UV-based assay developed for *myo*-inositol detection in animal feeds, foods, and other materials offer promising avenues for application in coral monitoring and restoration efforts.

Methods

Culture maintenance

Symbiodiniaceae cultures (*Breviolum minutum* ITS2: B1, culture ID: RT2, CCMP2463) originally isolated from *E. diaphana diaphana* were sub-cultured ($n = 5$) from existing stocks at the University of Technology Sydney by adding 10 mL of original cultures in 90 mL of autoclaved and filter sterilised (0.22 μ m) artificial seawater (ASW) and F/2 media. Cultures were grown for one month (to achieve a minimum cell density of 10^6 cells/mL) at 26 °C with an irradiance of 85 ± 15 μ mol photons $m^{-2} s^{-1}$ (Philips TLD 18 W/54 fluorescent tubes, 10,000 K on a 12 h:12 h light:dark cycle). Before

use, cells were centrifuged at $700 \times g$ for 10 min at 26 °C and rinsed twice with ASW to remove residual media solution. Cells were resuspended in 100 mL ASW + F/2 media in sterile culture flasks. Cell counts were conducted through flow cytometry for each Symbiodiniaceae subculture. Specifically, an aliquot of 100 μ L was collected from each 1 mL sample, diluted 1:10 and directly used for flow cytometry analysis (CytoFLEX S, Beckman Coulter, CA, United States). Symbiodiniaceae cells were identified according to their chlorophyll *a* fluorescence (650 nm) and subsequently enumerated. Sample blanks ($n = 4$) were run alongside, and their average number of events subtracted from each sample (blank correction). Symbiodiniaceae flow cytometer gating strategy is shown in Supplementary Fig. 4. Cell counts were used to calculate the volume needed for 50 mL of 20,000 cells/mL prior to metabolomics extraction.

E. diaphana (AIMS 4 genotype^{75,76}) were maintained in ASW, with 30–50 μ mol/m²/s¹ of light on a 12 h:12 h light:dark cycle and in water baths maintained at 26 °C \pm 0.5 °C. *E. diaphana* were provided with constant aeration to prevent oxygen depletion. *E. diaphana* were fed with freshly hatched *Artemia* nauplii twice weekly, with water changes occurring the day after feeding to manage water quality and ensure digestion of food. *E. diaphana* were starved for one week before experimentation and moved to experimental containers the day prior to experimentation to allow for attachment.

Scyllo-inositol-2-dehydrogenase detection

To identify whether *B. minutum* possesses scyllo-inositol-2-dehydrogenase, we conducted a BLAST search and a gene ortholog finder. For the BLAST search, we curated 22 known *Iol* genes in 7 species from NCBI (Supplementary Data 2). The protein blast identified four *B. minutum* candidate genes, with only one (“symbB.v1.2.001032”) passing the criteria of per cent identity >30%, per cent coverage >50% and *e*-value < $1e^{-5}$ using DIAMOND version 2.1.9⁷⁷. In gene orthologs among 15 species (Supplementary Data 2), Orthofinder version 2.5.5 resulted in 56,046 ortholog groups⁷⁸. Of these orthologs, three ortholog groups contained scyllo-inositol-2-dehydrogenase (Supplementary Data 2), which identified 5 potential *Iol* genes, including symbB.v1.2.008936, symbB.v1.2.008937, symbB.v1.2.001032, symbB.v1.2.040931, and symbB.v1.2.018378. Only symbB.v1.2.001032 appeared in both the BLAST and Orthofinder searches. It was present in all Symbiodiniaceae species examined, but not *Exaiptasia diaphana* (Supplementary Data 2).

Menthol bleaching

E. diaphana underwent a 5-week menthol treatment to render them aposymbiotic⁷⁹ as successfully implemented in previous metabolomics studies^{6,24}. *E. diaphana* were incubated in 0.19 mM final concentration of menthol (using a stock solution of 20% menthol w/v in 100% ethanol) for 5–7 h daily, before being rinsed and returned to ASW. Incubation occurred during the light cycle, and feeding occurred twice a week on days without menthol incubation. This process was repeated for 4 consecutive days, followed by a 3-day relief, and this pattern was repeated for 4 weeks. After 4 weeks of treatment, the final concentration was increased to 0.27 mM for 4 days to remove residual symbionts that had not yet been expelled. *E. diaphana* were confirmed symbiont-free using fluorescence microscopy (Nikon Ni Automated UPRIGHT Microscope) under an excitation band of 578 \pm 10.5 nm and an emission band of 641 \pm 37.5 nm with a magnification of 10 \times . Aposymbiotic *E. diaphana* were maintained in dark containers after the first week of menthol treatment under the same temperature, feeding, and aeration conditions as the symbiotic *E. diaphana*. Aposymbiotic *E. diaphana* were not treated with menthol and starved for one week prior to experimentation.

Heat stress exposure

Symbiodiniaceae cultures, aposymbiotic *E. diaphana*, and symbiotic *E. diaphana*, were exposed to a standardised heat stress design (Coral Bleaching Automated Stress System (CBASS))⁵⁸. Two water baths were used: one remained at a constant 26 °C, while the other followed the CBASS

acute heat treatment protocol⁵⁸. The heat treatment began at mid-light cycle, after 6 h of light at 26 °C, gradually increasing to 33 °C over three hours. The temperature was then maintained at 33 °C for an additional three hours before cooling back to 26 °C over one hour in the dark. Following this, samples remained at 26 °C in the dark for 11 more hours, bringing the total experiment duration to 24 h. This widely used and standardised heat stress assay allows for cross-comparison between studies⁸⁰.

Sampling for the initial heat stress experiment, which aimed to identify inositol isomers in Symbiodiniaceae cultures and both symbiotic and aposymbiotic cnidarians, occurred at three time points (Supplementary Fig. 1):

- T1: Mid-light phase, once the temperature reached 33 °C.
- T2: End of the light phase, after 3 h at 33 °C.
- T3: Dark phase, following the recovery period (after 12 h in the dark, 24 h total).

Lithium incubations

To determine the minimum concentration of lithium chloride that effectively blocks inositol transport in the cnidarian-algal symbiosis without causing harm to the organisms (measured via the typical stress proxy of symbiont photophysiology, F_v/F_m), Symbiodiniaceae cultures ($n = 3$) were incubated in several concentrations of lithium chloride based on concentrations previously used on *Hydra*, a freshwater cnidarian⁸¹. Lithium chloride was dissolved in ASW and added into Symbiodiniaceae cultures to reach final concentrations of 0.02, 0.05, 0.1, 0.2, 0.5, 1, 2 mM⁸¹. These samples were compared to a control without lithium chloride ($n = 3$). Incubations occurred for 96 h with daily measurements of photophysiological performance (see below; *Photophysiological sampling of Symbiodiniaceae*) at mid-light cycle. Samples were collected for inositol metabolite profiling at the end of the 96-hour incubation. Results demonstrated a concentration of 0.1 mM was the minimum to achieve significant changes in inositol concentrations without significantly affecting photophysiology (Supplementary Data 6).

Symbiotic *E. diaphana* ($n = 5$ biological replications, each consisting of 10 individuals) were used to investigate the role of inositols within the cnidarian-algal symbiosis. Following the results from incubations on Symbiodiniaceae cultures (Supplementary Data 6), a concentration of 0.1 mM lithium chloride dissolved in ASW was used. Incubation occurred for 96 h with photophysiological measurements (see below; *Photophysiological sampling of E. diaphana*) taken daily at mid-light cycle. Samples were collected for metabolite profiling at the end of the 96-h incubation. Treatments consisted of control temperatures (26 °C for 96 h) without and with 0.1 mM lithium, heat exposure (33 °C for 96 h) without and with 0.1 mM lithium ($n = 5$ open treatment, total $n = 20$).

Photophysiological sampling of Symbiodiniaceae

Photophysiological performance of Symbiodiniaceae was assessed using a Soliense LIFT (Light Induced Fluorescence Transient)-FRR (Fast Repetition Rate) fluorometer (LIFT-FRRf; Soliense Inc. USA)⁴⁹. All cultures were low light (ca. 5–10 μ mol photons m⁻² s⁻¹) acclimated for at least 30 min prior to measurements. An aliquot of 200 μ L for each culture replicate ($n = 5$, distinct samples) was transferred to the LIFT-FRRf optical chamber and diluted with 800 μ L ASW. Excitation was delivered using a blue LED excitation source (peak excitation 445 nm), delivering single turnover fluorescent transients of 100 flashlets of 1.6 μ s at 2.5 μ s, followed by 127 flashlets of 1.6 μ s. All fluorescence yields were adjusted for baseline fluorescence using ASW + F/2. Light response protocols were used to derive the maximum PSII photochemical efficiency (F_v/F_m , dimensionless) as a proxy for tracking cellular health, using a model describing the light dependency of PSII photochemistry (as per Suggett et al. 2022).

Photophysiological sampling of *E. diaphana*

To assess the photophysiological performance of symbiotic *E. diaphana* during the CBASS experiments without lithium incubations, the F_v/F_m was measured using the multi-taxa phenotyping (MTP) design⁸². The

MTP consists of two instruments, an Imaging PAM and a thermocycler (Abi Veriti), which allowed for the temperature conditions of the CBASS to be maintained throughout dark adaptation and sampling⁸². F_v/F_m measurements were taken after 15 min of dark adaptation (settings: actinic light: 3, shutter: 1, sensitivity: 50.2).

During the lithium incubations, the photophysiological health of *E. diaphana* ($n = 5$ per treatment per time point, distinct samples) were measured using MAXI Imaging PAM (Walz) (settings: light intensity: 3, measuring light frequency: 1, and actinic light: 4) placed over the containers in the water baths to maintain temperatures. This ensured limited handling of lithium-dosed samples. Measurements were taken daily in the middle of the light cycle.

Metabolite sampling and extractions

Samples were collected to quantify the inositol stereoisomers in Symbiodiniaceae cultures (free-living) and *in hospite* (symbiont pellets isolated from symbiotic *E. diaphana* via centrifugal separation – see below) and cnidarians without symbionts (aposymbiotic) and symbiotic host tissues (the host fractions of the separated *E. diaphana* – see below), and the relative changes in stereoisomer concentration during heat stress ($n = 5$ per species per treatment, distinct samples).

For Symbiodiniaceae cultures, 10^6 cells (based on flow cytometry counts above) were collected onto a 0.22 μm filter fitted with a vacuum pump, filters removed with tweezers and placed in cryovials, and samples snap frozen in liquid nitrogen. All equipment was rinsed with methanol and ultrapure water between each replicate, and to ensure no contamination between samples, a blank of ultrapure water was also run after every 5 replicates and extracted using the same methods outlined below. All samples were stored at -80°C until extraction.

All subsequent steps were performed at 4°C to prevent metabolite losses during extraction. Metabolite extractions, analysis and data processing are based on the methods described in Matthews et al.⁸³. To first remove residual salts (which affect GC-MS analysis), filtrates (including blank samples) were resuspended in 500 μL cold (4°C) ultrapure water and centrifuged at $3000 \times g$ for 5 min at 4°C . The supernatant was discarded, and pellets were frozen at -80°C for 1 h and lyophilised at -105°C for 18 h. The semi-polar metabolites were extracted by adding approximately 10 mg acid-washed glass beads to each pellet and 200 μL 100% cold (-20°C) methanol spiked with 20 $\mu\text{g}/\text{mL}$ final concentration of the internal standard D-sorbitol-6- ^{13}C , and cells were lysed using a bead mill at 50 Hz for 3 min. A further 800 μL of 100% cold methanol (+ IS) was added to each cell slurry, and samples were vortexed for exactly 1 min each. Cell debris was pelleted at $3000 \times g$ for 30 min at 4°C , and the supernatant collected. To each cell debris, a further 1 mL 50% cold (-20°C) methanol was added and samples vortexed for 30 s. Cell debris was pelleted at $3000 \times g$ for 30 min at 4°C , and the supernatant was combined with the 100% methanol extracts. Samples were centrifuged at $16,000 \times g$ for 15 min at 4°C , and $5 \times 50 \mu\text{L}$ (250 μL total volume) dried in a glass insert in a concentrator at 30°C .

Solid phase extractions (SPE) from 50 mL of culture media were performed to detect inositols excreted by Symbiodiniaceae cells. Samples were acidified to a pH of 2 with 20% HCl and added to Waters Oasis Columns (Oasis HLB 6 cc Vac Cartridge, 200 mg Sorbent per Cartridge) under a vacuum between 0 and 5 Hg to ensure a slow movement through the cartridges⁸⁴. Metabolites were then eluted from the cartridges using 75% methanol (with internal standard D-Sorbitol-6- ^{13}C at 5 μM).

Inositol isoforms were extracted from symbiotic and aposymbiotic *E. diaphana* based on methods described in Matthews et al.⁶. To ensure enough biomass for metabolite detection, $10 \times E. diaphana$ with an oral disk of between 2 and 4 mm were pooled for each replicate ($n = 5$ per treatment, distinct samples). At each sampling point (Supplementary Fig. 1), *E. diaphana* were collected from their incubations using a Pasteur pipette, the seawater removed, and the pooled *E. diaphana* were snap frozen in liquid nitrogen and stored at -80°C until further processing.

E. diaphana were rapidly homogenised with a mechanical saw-tooth homogeniser (IKA T10 BS5, ThermoFisher Scientific) for 1 min at a mid-

speed setting in 1 mL of cold (4°C) ultrapure water. Symbionts were pelleted by centrifugation ($2500 \times g$ for 5 min at 4°C), and the host supernatant was transferred to a new tube. Symbiont pellets were diluted with 1 mL of cold (4°C) ultrapure water, all samples vigorously vortexed for 1 min followed by a second centrifugation ($2500 \times g$ for 5 min at 4°C). For host samples, the host supernatant was transferred to a new tube, leaving any residual symbionts, and for symbiont pellets, the supernatant on the symbiont pellet was discarded. Subsamples ($n = 5$) of the host material were confirmed for Symbiodiniaceae absence by light microscopy (at $\times 40$ magnification). The cleaned host and symbiont fractions were frozen at -80°C for 1 h and lyophilised for 18 h at -105°C .

Metabolites were extracted from the dried symbiont pellets as above. For the *E. diaphana* host tissue, 1 mL of 100% methanol (-20°C) containing the internal standard D-Sorbitol-6- ^{13}C at 10 μM was added to ~ 30 mg of lyophilised host material to extract the semi-polar metabolites. The host fractions were sonicated for 30 min at 4°C in an ultrasonic bath and centrifuged ($3000 \times g$ for 30 min at 4°C), and the supernatant containing the extracted metabolites was collected and stored at -80°C . Extraction was then repeated with 1 mL of 50% MeOH (-20°C) to extract the polar fraction. Samples were then centrifuged ($3000 \times g$ for 30 min at 4°C) and the supernatant pooled with the first extract. The total extract was then further centrifuged at $16,100 \times g$ for 15 min at 4°C to ensure the removal of all particulates. Aliquots (total volume 200 μL) were then concentrated under vacuum (Eppendorf Concentrator 5301) at 30°C until dry. For data normalisation, the protein content of the pellet that remained after extractions was measured using a modified Bradford Assay⁸⁵.

Absolute quantification of inositol stereoisomers

Inositol analysis was performed using gas chromatography–mass spectrometry (GC/MS). Extracts were spiked with internal standard, sorbitol and derivatised using the following protocol: 20 μL N-methyl-N-(trimethylsilyl) trifluoroacetamide (MSTFA) was added and incubated at 37°C for 30 min, while agitating at 750 rpm. Derivatised samples were analysed using a GC-MS-QP2020 (Shimadzu Corporation, Kyoto, Japan) equipped with an AOC-20is autosampler (Shimadzu Corporation). The column used was an SH-Rxi-5Sil MS fused silica capillary column (30.0 m \times 0.25 mm \times 0.25 μm) operating in electron impact mode at 70 eV. Helium was used as the carrier gas at a constant flow of 1.0 mL min $^{-1}$ and an injection volume of 1 μL , with an injector temperature of 280°C and an ion source temperature of 230°C . The oven temperature was programmed for a gradient of 50°C (held for 2 min) to 220°C ($4^\circ\text{C}/\text{min}$); 220°C to 300°C ($60^\circ\text{C}/\text{min}$) and held for 3 min. Mass spectra were obtained in the selective ion monitoring (SIM) mode. The quantitative ions for *myo*-, *scyllo*- and *chiro* inositol were m/z 305, 318 and 305, respectively. Inositol peaks were identified by comparison of their retention times with analytical standards (Fig. S5) and quantified using 7-point calibration curves.

Targeted GC/MS metabolite profiling analysis of *E. diaphana*

For metabolite profiling of lithium-dosed *E. diaphana*, both host and symbiont metabolite extracts were prepared as above from the four treatments (Control and heat stress, both with and without lithium, $n = 5$ per treatment per species, distinct samples). Dried samples ($3 \times 75 \mu\text{L}$ aliquots dried in a glass insert, total 225 μL) were derivatised online using the Shimadzu AOC6000 autosampler robot. Derivatisation was achieved by adding 25 μL of methoxyamine hydrochloride (30 mg/mL in Pyridine), followed by shaking at 37°C for 2 h. Samples were then derivatised with 25 μL of N,O-bis (Trimethylsilyl)trifluoroacetamide (BSTFA) with 1% Trimethylchlorosilane (TMCS) (Thermo Scientific) for 1 h at 37°C . The sample was left for 1 h before 1 μL was injected onto the GC column using a hot needle technique. Split (1:10) injections were done for each sample. The GC-MS system used consisted of an AOC6000 autosampler, a 2030 Shimadzu gas chromatograph and a TQ8040 quadrupole mass spectrometer (Shimadzu, Japan). The mass spectrometer was tuned according to the manufacturer's recommendations using tris-

(perfluorobutyl)-amine (CF43). GC-MS was performed on a 30 m Agilent DB-5 column with 1 µm film thickness and 0.25 mm internal diameter. The injection temperature (Inlet) was set at 280 °C, the MS transfer line at 280 °C and the ion source adjusted to 200 °C. Helium was used as the carrier gas at a flow rate of 1 mL/min, and Argon gas was used as the collision cell gas to generate the MRM product ion. The analysis of the derivatised samples was performed under the following temperature programme; start at injection 100 °C, a hold for 4 min, followed by a 10 °C min⁻¹ oven temperature ramp to 320 °C following a final hold for 11 min. Approximately 520 quantifying multiple reaction monitoring (MRM) targets were collected using Shimadzu Smart Database, along with a qualifier for each target, which covers about 350 endogenous metabolites and multiple ¹³C labelled internal standards. Both chromatograms and MRMs were evaluated using the Shimadzu GC-MS browser and LabSolutions Insight software.

Metabolite profiling data analysis

Metabolite profile data of the lithium-dosed experiment were normalised to the peak area of the internal standard D-sorbitol-6-¹³C and then to the protein content of the cell debris pellet⁸³. Data were filtered using a relative standard deviation threshold of 40%, yielding 100 metabolites in host tissues and 88 metabolites in symbiont cells (Supplementary Data 7 and 8). To test for overall differences in metabolite pools between treatments, statistical analyses (described below) were performed using MetaboAnalyst 6.0⁸⁶, where data were tested for normality and homogeneity, before being log-transformed and mean-centred. Data were visualised using Principal Component Analysis (PCA) computed using the Euclidean distance based on PCs 1 and 2 and PERMANOVA. Multivariate (ANOVA) and Fisher's LSD were performed on the samples collected after 96 h to identify individual metabolites that varied significantly between the heat stress and control treatments, both with and without lithium. Statistically different metabolites were determined based on a False Discovery Rate (FDR) corrected significance value ($p_{\text{adj}} < 0.05$). The statistically different metabolites were used to construct heatmaps based on normalised, autoscaled data. Samples were clustered according to similarity in expression profiles using Ward's method, while metabolites were clustered using the Euclidean distance metric.

Statistics and reproducibility

Cell count data were recorded using CytExpert Version 2.4. Mass spectra were collected electronically using a GC-MS-QP2020 (Shimadzu Corporation, Kyoto, Japan) equipped with an AOC-20is autosampler (Shimadzu Corporation) or AOC6000 autosampler, a 2030 Shimadzu gas chromatograph and a TQ8040 quadrupole mass spectrometer (Shimadzu, Japan). Photophysiology was collected on a Soliense LIFT (Light Induced Fluorescence Transient)-FRR (Fast Repetition Rate) fluorometer (LIFT-FRR; Soliense Inc. USA) or MAXI Imaging PAM (Walz). Statistics were carried out in R v4.1.1⁸⁷, and Metaboanalyst 6.0⁸⁶. Packages used in R were ggplot2 v3.5.1, dplyr v1.1.4, and car v3.1.

Reporting summary

Further information on research design is available in the Nature Portfolio Reporting Summary linked to this article.

Data availability

The raw mass spectral data reported is available in Zenodo (10.5281/zenodo.14053065)⁸⁸. All other raw data is available as Supplementary Data.

Code availability

The code used in this work is publicly available and will be publicly maintained and updated at <https://github.com/JenMatthews/CoralInositols>.

Received: 7 November 2024; Accepted: 6 May 2025;

Published online: 15 May 2025

References

- Rädecker, N. et al. Heat stress destabilizes symbiotic nutrient cycling in corals. *Proc. Natl Acad. Sci. USA* **118**, e2022653118 (2021).
- Hillyer, K. E., Dias, D. A., Lutz, A., Roessner, U. & Davy, S. K. Exploring the coral bleaching tipping point with ¹³C metabolomics. In *Applied Environmental Metabolomics* (eds. Beale, D. J., Hillyer, K. E., Warden, A. C. & Jones, O. A. H.) 199–209 (Academic Press, 2022).
- Burriesci, M. S., Raab, T. K. & Pringle, J. R. Evidence that glucose is the major transferred metabolite in dinoflagellate–cnidarian symbiosis. *J. Exp. Biol.* **215**, 3467–3477 (2012).
- Hillyer, K. E., Dias, D., Lutz, A., Roessner, U. & Davy, S. K. ¹³C metabolomics reveals widespread change in carbon fate during coral bleaching. *Metabolomics* **14**, 12 (2018).
- Hillyer, K. E., Dias, D. A., Lutz, A., Roessner, U. & Davy, S. K. Mapping carbon fate during bleaching in a model cnidarian symbiosis: the application of ¹³C metabolomics. *N. Phytol.* **214**, 1551–1562 (2017).
- Matthews, J. L. et al. Optimal nutrient exchange and immune responses operate in partner specificity in the cnidarian–dinoflagellate symbiosis. *Proc. Natl Acad. Sci. USA* **114**, 13194–13199 (2017).
- Klueter, A., Crandall, J., Archer, F., Teece, M. & Coffroth, M. Taxonomic and environmental variation of metabolite profiles in marine dinoflagellates of the genus *Symbiodinium*. *Metabolites* **5**, 74–99 (2015).
- Yu, X. et al. Metabolic and immune costs balance during natural acclimation of corals in fluctuating environments. *Mar. Environ. Res.* **193**, 106284 (2024).
- Leinbach, S. E., Speare, K. E., Rossin, A. M., Holstein, D. M. & Strader, M. E. Energetic and reproductive costs of coral recovery in divergent bleaching responses. *Sci. Rep.* **11**, 23546 (2021).
- Leuzinger, S., Willis, B. L. & Anthony, K. R. N. Energy allocation in a reef coral under varying resource availability. *Mar. Biol.* **159**, 177–186 (2012).
- Nunn, B. L. et al. Resilience in a time of stress: revealing the molecular underpinnings of coral survival following thermal bleaching events. Preprint at *bioRxiv* <https://doi.org/10.1101/2024.04.02.587798> (2024).
- Anderson, L. The cyclitols. In *The Carbohydrates* 519–579 (Academic Press, 1972).
- Hoffmann-Ostenhof, O. & Pittner, F. The biosynthesis of myo-inositol and its isomers. *Can. J. Chem.* **60**, 1863–1871 (1982).
- Berridge, M. J. & Irvine, R. F. Inositol phosphates and cell signalling. *Nature* **341**, 197–205 (1989).
- Turner, B. L., Papházy, M. J., Haygarth, P. M. & McKelvie, I. D. Inositol phosphates in the environment. *Philos. Trans. R. Soc. Lond. B* **357**, 449–469 (2002).
- Michell, R. H. Inositol derivatives: Evolution and functions. *Nat. Rev. Mol. Cell Biol.* **9**, 151–161 (2008).
- Tsim, S.-T., Wong, J. T. Y. & Wong, Y. H. Calcium ion dependency and the role of inositol phosphates in melatonin-induced encystment of dinoflagellates. *J. Cell Sci.* **110**, 1387–1393 (1997).
- Healy, M. E., Dillavou, C. L. & Taylor, G. E. Diagnostic medium containing inositol, urea, and caffeic acid for selective growth of *Cryptococcus neoformans*. *J. Clin. Microbiol.* **6**, 387–391 (1977).
- Xue, C. et al. Role of an expanded inositol transporter repertoire in *Cryptococcus neoformans* sexual reproduction and virulence. *mBio* **1**, e00084–10 (2010).
- Chen, X., Zhang, B., Li, H. & Peng, X. Myo-inositol improves the host's ability to eliminate balofloxacin-resistant *Escherichia coli*. *Sci. Rep.* **5**, 10720 (2015).
- Koch, E. J., Moriano-Gutierrez, S., Ruby, E. G., McFall-Ngai, M. & Liebecke, M. The impact of persistent colonization by *Vibrio fischeri* on the metabolome of the host squid *Euprymna scolopes*. *J. Exp. Biol.* **223**, jeb212860 (2020).

22. Vilchez, J. I. et al. DNA demethylases are required for myo-inositol-mediated mutualism between plants and beneficial rhizobacteria. *Nat. Plants* **6**, 983–995 (2020).
23. Kennedy-Mendez, A. *Characterization of Pinitol Catabolism in Sinorhizobium Meliloti and its Role in Nodule Occupancy*. Western Michigan University, Masters Theses (2018).
24. Matthews, J. L. et al. Partner switching and metabolic flux in a model cnidarian–dinoflagellate symbiosis. *Proc. R. Soc. B.* **285**, 20182336 (2018).
25. Ochsenkühn, M. A., Röthig, T., D’Angelo, C., Wiedenmann, J. & Voolstra, C. R. The role of floridoside in osmoadaptation of coral-associated algal endosymbionts to high-salinity conditions. *Sci. Adv.* **3**, e1602047 (2017).
26. Boehning, D., van Rossum, D. B., Patterson, R. L. & Snyder, S. H. A peptide inhibitor of cytochrome c/inositol 1,4,5-trisphosphate receptor binding blocks intrinsic and extrinsic cell death pathways. *Proc. Natl Acad. Sci. USA* **102**, 1466–1471 (2005).
27. Chakraborty, S. et al. Potential sabotage of host cell physiology by apicomplexan parasites for their survival benefits. *Front. Immunol.* **8**, 1261 (2017).
28. Verma, S. C. & Miyashiro, T. Quorum sensing in the squid–vibrio symbiosis. *Int. J. Mol. Sci.* **14**, 16386–16401 (2013).
29. Oldroyd, G. E. D. & Downie, J. A. Calcium, kinases and nodulation signalling in legumes. *Nat. Rev. Mol. Cell Biol.* **5**, 566–576 (2004).
30. Ashley, I. A. et al. Genomic conservation and putative downstream functionality of the phosphatidylinositol signalling pathway in the cnidarian–dinoflagellate symbiosis. *Front. Microbiol.* **13**, 1094255 (2023).
31. Ebrahimzadeh, Z. et al. A pan-apicomplexan phosphoinositide-binding protein acts in malarial microneme exocytosis. *EMBO Rep.* **20**, e47102 (2019).
32. Leirião, P. et al. HGF/MET signalling protects Plasmodium-infected host cells from apoptosis. *Cell. Microbiol.* **7**, 603–609 (2005).
33. McNamara, C. W. et al. Targeting Plasmodium PI(4)K to eliminate malaria. *Nature* **504**, 248–253 (2013).
34. Sproles, A. E. et al. Phylogenetic characterization of transporter proteins in the cnidarian–dinoflagellate symbiosis. *Mol. Phylogenet. Evol.* **120**, 307–320 (2018).
35. Lehnert, E. M. et al. Extensive differences in gene expression between symbiotic and aposymbiotic cnidarians. *G3 Genes, Genomes, Genet.* **4**, 277–295 (2014).
36. Rosic, N. et al. Unfolding the secrets of coral–algal symbiosis. *ISME J.* **9**, 844–856 (2015).
37. Weston, A. J. et al. Proteomics links the redox state to calcium signaling during bleaching of the scleractinian coral *Acropora microphthalma* on exposure to high solar irradiance and thermal stress[S]. *Mol. Cell. Proteom.* **14**, 585–595 (2015).
38. Bellantuono, A. J., Dougan, K. E., Granados-Cifuentes, C. & Rodriguez-Lanetty, M. Transcriptome landscape of a thermal-tolerant coral endosymbiont reveals molecular signatures of symbiosis and dysbiosis. *bioRxiv* <https://doi.org/10.1101/508184> (2018).
39. Maor-Landaw, K., van Oppen, M. J. H. & McFadden, G. I. Symbiotic lifestyle triggers drastic changes in the gene expression of the algal endosymbiont *Brevium minutum* (Symbiodiniaceae). *Ecol. Evol.* **10**, 451–466 (2020).
40. Haydon, T. D. et al. Metabolomic signatures of corals thriving across extreme reef habitats reveal strategies of heat stress tolerance. *Proc. R. Soc. B Biol. Sci.* **290**, 20221877 (2023).
41. González-Pech, R. A. et al. Physiological factors facilitating the persistence of *Pocillopora aliciae* and *Plesiastrea versipora* in temperate reefs of south-eastern Australia under ocean warming. *Coral Reefs* **41**, 1239–1253 (2022).
42. Hager, K. et al. Kinetics and specificity of the renal Na⁺/myo-inositol cotransporter expressed in *Xenopus* Oocytes. *J. Membr. Biol.* **143**, 103–113 (1995).
43. Uldry, M. et al. Identification of a mammalian H⁺-myo-inositol symporter expressed predominantly in the brain. *EMBO J.* **20**, 4467 (2001).
44. Coady, M. J., Wallendorff, B., Gagnon, D. G. & Lapointe, J.-Y. Identification of a novel Na⁺/myo-inositol cotransporter *. *J. Biol. Chem.* **277**, 35219–35224 (2002).
45. Wright, E. M. & Turk, E. The sodium/glucose cotransport family SLC5. *Pflug. Arch. Eur. J. Physiol.* **447**, 510–518 (2004).
46. *Arabidopsis INOSITOL TRANSPORTER2 Mediates H⁺ Symport of Different Inositol Epimers and Derivatives across the Plasma Membrane* | *Plant Physiology* | Oxford Academic. (2007) <https://academic.oup.com/plphys/article/145/4/1395/6107234>.
47. Lancôt, C. M. et al. Physiological stress response of the scleractinian coral *Stylophora pistillata* exposed to polyethylene microplastics. *Environ. Pollut.* **263**, 114559 (2020).
48. Schneider, S. Inositol transport proteins. *FEBS Lett.* **589**, 1049–1058 (2015).
49. Lehnert, E. M., Burriesci, M. S. & Pringle, J. R. Developing the anemone *Aiptasia* as a tractable model for cnidarian–dinoflagellate symbiosis: the transcriptome of aposymbiotic *A. pallida*. *BMC Genomics* **13**, 271 (2012).
50. Matthews, J. L. et al. Menthol-induced bleaching rapidly and effectively provides experimental aposymbiotic sea anemones (*Aiptasia* sp.) for symbiosis investigations. *J. Exp. Biol.* **219**, 306–310 (2016).
51. Thornhill, D. J., Xiang, Y., Pettay, D. T., Zhong, M. & Santos, S. R. Population genetic data of a model symbiotic cnidarian system reveal remarkable symbiotic specificity and vectored introductions across ocean basins. *Mol. Ecol.* **22**, 4499–4515 (2013).
52. Wang, J.-T., Chen, Y.-Y., Tew, K. S., Meng, P.-J. & Chen, C. A. Physiological and biochemical performances of menthol-induced aposymbiotic corals. *PLoS ONE* **7**, e46406 (2012).
53. Weis, V. M., Davy, S. K., Hoegh-Guldberg, O., Rodriguez-Lanetty, M. & Pringle, J. R. Cell biology in model systems as the key to understanding corals. *Trends Ecol. Evol.* **23**, 369–376 (2008).
54. Matthews, J. L. et al. Coral endosymbiont growth is enhanced by metabolic interactions with bacteria. *Nat. Commun.* **14**, 6864 (2023).
55. Baumgarten, S. et al. The genome of *Aiptasia*, a sea anemone model for coral symbiosis. *Proc. Natl Acad. Sci. USA* **112**, 11893–11898 (2015).
56. Ying, H. et al. The whole-genome sequence of the coral *Acropora millepora*. *Genome Biol. Evol.* **11**, 1374–1379 (2019).
57. Shinzato, C. et al. Using the *Acropora digitifera* genome to understand coral responses to environmental change. *Nature* **476**, 320–323 (2011).
58. Voolstra, C. R. et al. Standardized short-term acute heat stress assays resolve historical differences in coral thermotolerance across microhabitat reef sites. *Glob. Chang. Biol.* **26**, 4328–4343 (2020).
59. Suggett, D. J. et al. Functional diversity of photobiological traits within the genus *Symbiodinium* appears to be governed by the interaction of cell size with cladal designation. *N. Phytol.* **208**, 370–381 (2015).
60. Klages, K., Boldingh, H. & Smith, G. S. Accumulation of myo-inositol in *Actinidia* seedlings subjected to salt stress. *Ann. Bot.* **84**, 521–527 (1999).
61. Yancey, P. H., Rhea, M. D., Kemp, K. & Bailey, D. M. Trimethylamine oxide, betaine and other osmolytes in deep-sea animals: depth trends and effects on enzymes under hydrostatic pressure. *Cell. Mol. Biol.* **50**, 371–376 (2004).
62. Yancey, P. H. et al. Betaines and Dimethylsulfoniopropionate as major osmolytes in Cnidaria with endosymbiotic dinoflagellates. *Physiol. Biochem. Zool.* **83**, 167–173 (2010).
63. Downing, A. B., Wallace, G. T. & Yancey, P. H. Organic osmolytes of amphipods from littoral to hadal zones: Increases with depth in trimethylamine N-oxide, scyllo-inositol and other potential pressure counteractants. *Deep Sea Res. Part I: Oceanogr. Res. Pap.* **138**, 1–10 (2018).

64. Nikitashina, V., Stettin, D. & Pohnert, G. Metabolic adaptation of diatoms to hypersalinity. *Phytochemistry* **201**, 113267 (2022).
65. Tejima, K., Arima, Y., Yokoyama, T. & Sekimoto, H. Composition of amino acids, organic acids, and sugars in the peribacteroid space of soybean root nodules. *Soil Sci. Plant Nutr.* **49**, 239–247 (2003).
66. Campbell, I. H., Campbell, H. & Smith, D. J. Insulin signaling as a therapeutic mechanism of lithium in bipolar disorder. *Transl. Psychiatry* **12**, 1–8 (2022).
67. Sade, Y. et al. IP3 accumulation and/or inositol depletion: two downstream lithium's effects that may mediate its behavioral and cellular changes. *Transl. Psychiatry* **6**, e968 (2016).
68. Rådecker, N., Escrig, S., Spangenberg, J. E., Voolstra, C. R. & Meibom, A. Coupled carbon and nitrogen cycling regulates the cnidarian–algal symbiosis. *Nat. Commun.* **14**, 6948 (2023).
69. Chen, X., Wang, J. & Zhao, W. Effects of dietary inositol supplementation on growth, digestive performance, antioxidant capacity, and body composition of golden pompano (*Trachinotus ovatus*). *Front. Physiol.* **13**, 850470 (2022).
70. Bu, X. et al. Effects of myo-inositol on growth performance, body composition, antioxidant status, non-specific immunity and lipid metabolism of juvenile Chinese mitten crab (*Eriocheir sinensis*). *Aquac. Nutr.* **26**, 1623–1635 (2020).
71. Fenili, D., Brown, M., Rappaport, R. & McLaurin, J. Properties of scyllo-inositol as a therapeutic treatment of AD-like pathology. *J. Mol. Med.* **85**, 603–611 (2007).
72. Ochsenkühn, M. A., Schmitt-Kopplin, P., Harir, M. & Amin, S. A. Coral metabolite gradients affect microbial community structures and act as a disease cue. *Commun. Biol.* **1**, 1–10 (2018).
73. Bartels, N. et al. Paired metabolomics and volatilomics provides insight into transient high light stress response mechanisms of the coral *Montipora mollis*. *Metabolomics* **20**, 66 (2024).
74. Mashini, A. G. et al. The Influence of Symbiosis on the Proteome of the *Exaiptasia Endosymbiont Brevium minutum*. *Microorganisms* **11**, 292 (2023).
75. Tortorelli, G., Belderok, R., Davy, S. K., McFadden, G. I. & van Oppen, M. J. H. Host genotypic effect on algal symbiosis establishment in the coral model, the anemone *Exaiptasia diaphana*, from the Great Barrier Reef. *Front. Mar. Sci.* **6**, 833 (2020).
76. Dungan, A. M. et al. *Exaiptasia diaphana* from the Great Barrier Reef: a valuable resource for coral symbiosis research. *Symbiosis* **80**, 195–206 (2020).
77. Buchfink, B., Reuter, K. & Drost, H.-G. Sensitive protein alignments at tree-of-life scale using DIAMOND. *Nat. Methods* **18**, 366–368 (2021).
78. Emms, D. M. & Kelly, S. OrthoFinder: phylogenetic orthology inference for comparative genomics. *Genome Biol.* **20**, 238 (2019).
79. Matthews, J. L. et al. Menthol-induced bleaching rapidly and effectively provides experimental aposymbiotic sea anemones (*Aiptasia* sp.) for symbiosis investigations. *J. Exp. Biol.* <https://doi.org/10.1242/jeb.128934> (2015).
80. Voolstra, C. R. et al. Standardized methods to assess the impacts of thermal stress on Coral Reef Marine Life. *Ann. Rev. Mar. Sci.* **17**, 193–226 (2025).
81. Pachghare, V., Chandra, M., Surve, A. & Kulkarni, A. Evaluating toxicity of lithium to *Hydra viridissima*. *Proc. Natl Acad. Sci. India, Sect. B Biol. Sci.* <https://doi.org/10.1007/s40011-023-01488-x> (2023).
82. England, H. et al. A portable multi-taxa phenotyping device to retrieve physiological performance traits. *Sci. Rep.* **14**, 21826 (2024).
83. Matthews, J. L., Bartels, N., Doornun, S. N. E., Davy, S. K. & Souza, D. P. D. Gas chromatography-mass spectrometry-based targeted metabolomics of hard coral samples. *J. Vis. Exp.* <https://doi.org/10.3791/65628> (2023).
84. Dittmar, T., Koch, B., Hertkorn, N. & Kattner, G. A simple and efficient method for the solid-phase extraction of dissolved organic matter (SPE-DOM) from seawater. *Limnol. Oceanogr. Methods* **6**, 230–235 (2008).
85. Bradford, M. M. A rapid and sensitive method for the quantitation of microgram quantities of protein utilizing the principle of protein-dye binding. *Anal. Biochem.* **72**, 248–254 (1976).
86. Pang, Z. et al. MetaboAnalyst 6.0: towards a unified platform for metabolomics data processing, analysis and interpretation. *Nucleic Acids Res.* **52**, W398–W406 (2024).
87. *R: A Language and Environment for Statistical Computing* (R Core Team, 2021).
88. Turner, L., Raina, J.-B., Kuzhiumparambil, U., Songsomboon, K. & Matthews, J. Inhibiting inositol transport disrupts metabolite profiles and mimics heat stress in a model cnidarian-Symbiodiniaceae symbiosis. [Metabolomics data files]. *Zenodo* <https://doi.org/10.5281/zenodo.14053064>.

Acknowledgements

We thank Taisia Lapshina for her help with GC-MS analyses. J.L.M. was supported by a University of Technology Sydney Chancellor's Fellowship.

Author contributions

J.L.M., J.B.R., and L.T. designed the study; L.T., U.K. and K.S. performed the experiments. J.L.M. analysed the data; L.T. and J.L.M. wrote the article with contributions from all coauthors.

Competing interests

The authors declare no competing interests.

Additional information

Supplementary information The online version contains supplementary material available at <https://doi.org/10.1038/s42003-025-08182-w>.

Correspondence and requests for materials should be addressed to Jennifer L. Matthews.

Peer review information *Communications Biology* thanks Sabrina Rosset and the other anonymous reviewer(s) for their contribution to the peer review of this work. Primary Handling Editors: Linn Hoffmann and Michele Repetto. A peer review file is available.

Reprints and permissions information is available at <http://www.nature.com/reprints>

Publisher's note Springer Nature remains neutral with regard to jurisdictional claims in published maps and institutional affiliations.

Open Access This article is licensed under a Creative Commons Attribution-NonCommercial-NoDerivatives 4.0 International License, which permits any non-commercial use, sharing, distribution and reproduction in any medium or format, as long as you give appropriate credit to the original author(s) and the source, provide a link to the Creative Commons licence, and indicate if you modified the licensed material. You do not have permission under this licence to share adapted material derived from this article or parts of it. The images or other third party material in this article are included in the article's Creative Commons licence, unless indicated otherwise in a credit line to the material. If material is not included in the article's Creative Commons licence and your intended use is not permitted by statutory regulation or exceeds the permitted use, you will need to obtain permission directly from the copyright holder. To view a copy of this licence, visit <http://creativecommons.org/licenses/by-nc-nd/4.0/>.

© The Author(s) 2025